Nitrogen-doped biochar fiber with graphitization from *Boehmeria nivea* for promoted peroxymonosulfate activation and non-radical degradation pathways with enhancing electron transfer

Shujing Ye [a], Guangming Zeng [a, *], Xiaofei Tan [a,*], Haipeng Wu [a, b, *], Jie Liang [a], Biao Song [a], Ning Tang [a], Peng Zhang [a], Yuanyuan Yang [a], Qiang Chen [a], Xiaopei Li [a]

[a] College of Environmental Science and Engineering, Hunan University and Key Laboratory of Environmental Biology and Pollution Control (Hunan University), Ministry of Education, Changsha 410082, PR China

[b] School of Hydraulic Engineering, Changsha University of Science & Technology, Changsha 410114, PR China

* Corresponding authors: Tel.: +86–731–88822754; fax: +86–731–88823701. Email address: zgming@hnu.edu.cn (Guangming Zeng), tanxf@hnu.edu.cn (Xiaofei Tan) wuhaipeng0701@126.com (Haipeng Wu).

ABSTRACT

Advanced oxidation has great promise in the degradation of organic pollutants, but the high preparation requirements, adjustment difficulty, high cost, potential hazard, and low repeatability of catalysts limit the practical applications of this technology. In this study, a metal-free biochar-based catalyst derived from biomass fiber was prepared assisted by graphitization and nitrogen incorporation (PGBF-N). The heterogeneous catalysis of peroxymonosulfate (PMS) was triggered by PGBF-N with degradation rate 7 times higher than that of pristine biochar. The high catalytic efficiency was attributed to the accelerated electron transfer originated from the high degree of graphitization and nitrogen functionalization of PGBF-N, in which the non-radical pathways containing carbon-bridge and singlet oxygen-mediated oxidation were elucidated as the predominant pathways for tetracycline degradation, instead of the dominant role of radical pathway in pristine biochar. Vacancies and defective edges formed on sp^2-hybridized carbon framework as well as the nitrogen doping sites and ketonic group of PGNF-N were considered as possible active sites. The excellent degradation rate in actual water indicated that the PGBF-N/PMS system dominated by non-radical pathway exhibited a high anti-interference ability to surrounding organic or inorganic compounds. This study provides a facile protocol for converting biomass fiber into functional catalyst and enables underlying insight in mediating dominated degradation mechanism of heterogeneous catalysis by biochar fiber.

Keywords: Biochar fiber; Advanced oxidation processes; Catalytic degradation; Electron transfer; Non-radical pathway; Water treatment

1. Introduction

Sulfate radical-based advanced oxidation processes (SR-AOPs) have been suggested as an effective approach to degrade persistent organic pollutants by scission of the peroxide O–O bond of peroxymonosulfate (PMS) or persulfate (PS) [1-3], with the longer half-life (30–40 μS) and higher redox potential (E^o = 2.5–3.1 V) of $SO_4^{\bullet -}$ than that of •OH. Metal-free carbon materials exhibit great potential as green alternatives of catalysts for heterogeneous catalytic reactions in SR-AOPs [4-6], owing to the following merits: no-metal leaching, acid-base resistance, biocompatibility, restorability, and versatility [7-11]. Carbocatalyst containing carbon basal plane with delocalized π-electrons, electron-rich functional group, and carbon in the form of π-π*, could hold the post of electron donors and regulators in the activation process [11, 12]. Graphene oxide and its reduced derivatives were synthesized by thermal annealing (rGO-CM), chemical reduction of hydrazine hydrate (rGO-HH), and hydrothermal reaction of ammonia solution (rGO-HT), respectively, and the best PMS activation was observed by rGO-HT which showed the highest content of ketonic group (C=O) [12]. Theoretical evidences revealed that the boundary defects like zigzag/armchair edges and vacancies can be considered as the active sites for O–O bond cleavage in PMS [12].

Besides the generation of free radicals to attack pollutants in SR-AOPs [13, 14], non-radical activation pathways, including the singlet-oxygen-mediated oxidation [15-18] and carbocatalyst-bridged mechanism (carbonaceous material acting as a

bridge for facilitating electron transfer from organic pollutants to the metastable PS/PMS without any reactive species production) [19-21], have been attracting increasing attention. Non-radical activation pathways show several remarkable advantages including: 1) enhancing anti-interference to organics and inorganics in the environmental background [15]; 2) avoiding radical self-quenching by propagation reaction [22]; and 3) fully utilizing the oxidized capacity of the oxidant. It is obvious that increasing the contribution of non-radical activation pathway in activating PS/PMS for pollutant degradation is one of the potential ways to further improve the performance of SR-AOP technology in practical application.

The initiation of the catalytic process requires a high concentration of electron cluster density. Electron accelerated transfer and heteroatom doping can induce the electron reconfiguration in unique electronic circumstance, which are treated as theoretically feasible approaches for the formation of activated state of PS/PMS and generation of reactive species. Incorporating heteroatom into carbon lattice could enhance the extent of charge delocalization thereby break the inertness of network structure of sp^2-hybridized carbon. Nitrogen doping is one of the most facile and promising approaches to strengthen the reactivity of catalyst, since the N with localized unpaired electrons is capable of 1) improving the electron density of the neighboring carbon atoms; 2) enhancing the π-electrons flow in sp^2-carbon by conjugation [23]; 3) generating more functional groups and defects; and 4) increasing the surface polarity of the carbon material for attractive interaction with the polar adsorbates. Chen et al.

synthesized a series of graphene with different N bonding configurations controlled delicately by regulating thermal annealing temperature to illustrate the role of Lewis basic sites with lone-pair electrons and graphitic N with higher electronegativity for disrupting the inertness of graphitic (sp^2-bonding carbon) network [23].

Since the commonly used carbon precursors for carbocatalyst (e.g., fullerene, graphene (oxide), carbon nanotubes) preparation are relatively expensive, ecologically toxic, and difficult for scale-up, it is desirable to develop a promising metal-free carbon material by applying low-cost and widespread carbon precursors such as biomass wastes [24-26]. However, the complex components in pristine biochar, as well as the disordered structure of amorphous carbon, cannot effectively realize the directional transfer of electrons. A more regular carbon configuration (sp^2-hybridized carbon) with high degree of graphitization is of great importance, otherwise heteroatom doping only increases the disorder and uncontrollable structure of the resulting biochar. Carbon materials with high graphitization and favorable functional groups are open frameworks to be decorated, which show excellent electrochemical characteristics and porous structure, drawing huge deal of scientific interests in the field of energy storage [27-30] and environmental remediation [31-34]. For example, highly graphitic biochar self-assembled with *g*-MoS_2 nanosheets was synthesized by our group to exhibit an outstanding activity in photodegradation [35]. The increasing degradation rate could be ascribed to the larger accessible surface areas for avoiding nanosheet agglomeration and the superior electrical conductivity for promoting electron transport.

Biomass fiber, collected from Ramie (*Boehmeria nivea* (L.) Gaud.), has the advantage of wide distribution, relatively simple constituent (mostly cellulose) and internal special ultra-fine pore structure, and it can be used as carbon precursor to obtain fiber-like activated biochar with chemical stability, large surface area, flexibility, and excellent electrical performance [36-38]. In order to facilitate electron transfer of biochar-based catalyst for PMS activation, especially the non-radical activation, a graphitic biochar fiber (PGBF) with unique structural and electronic characteristics was first synthesized via an efficient and green template-free route with K_2FeO_4. On this basis, doping N element into PGBF (PGBF-N) was conducted to create an electron-abundant circumstance, modulated functional groups and defective sites for PMS activation. Biochar fiber with abundant free flowing π-electrons on graphitization structure works as an excellent electron-bridge to accelerate electron transfer, and the doped nitrogen with lone pair electron and higher electronegativity could further activate electron flow and electron reconfiguration with the adsorbed PMS molecule. Tetracycline (TC) posing amphoteric behavior [39-41], a frequently detected antibiotic in water, was used as a representative to evaluate the effects of the as-prepared carbocatalyst in PMS system. The key purposes of this research are to 1) synthesize a series of metal-free biochar-based catalysts derived from biomass fiber by facile operation and characterize their structure and electrical properties; 2) explore the importance of graphitization and nitrogen doping on regulating dominant pathways; 3) analyze the active sites of the prepared biochar fiber in PMS activation for pollutant

degradation; and 4) discuss the degradation mechanisms.

2. Materials and methods

2.1 Materials

Ramie was provided by a local Ramie Institute of Hunan Agricultural University in China. Tetracycline (TC: purity >98.5%), potassium ferrate (K_2FeO_4), were purchased from Sigma-Aldrich, and were used without purification. Urea (CH_4N_2O), Oxone® (as $2KHSO_5 \cdot KHSO_4 \cdot K_2SO_4$, Alfa Aesar) were provided by Shanghai Macklin Biochemical Co., Ltd. In addition, the solutions were prepared using deionized water (18.25 MΩ cm) that produced by an Ulupure (UPRI-10 T) laboratory water system.

2.2 Biochar-based catalyst synthesis

Raw silk reeled off from Ramie bark was treated as biomass fiber (Scheme 1). The obtained biochar was successively subjected to dipping with K_2FeO_4 (0.1 M) at solid-to-liquid ratio of 1 g: 100 mL, grinding with urea at the mass ratio of 1: 2, calcining at temperatures of 900 ℃ and acid washing, which was named as PGBF-N. For comparison, the black solids obtained from above operation but without K_2FeO_4 soaking, nitrogen doping or both were denoted as BF-N, PGBF or BF, respectively. The synthesis details and characterization methods were provided in Supporting Information (SI).

2.3 Catalytic Degradation Experiments

The catalytic degradation performance of samples was carried out in a 250 mL

brown bottle in a thermostatic shaker with a shaking rate at 160 rpm. In a typical process, 10 mg of carbocatalyst was suspended in a 100 mL of TC solution (C_0=20 mg/L) for 30 min to establish the adsorption-desorption equilibrium (pre-experiment was carried out for 24 h and confirmed that the equilibrium state of adsorption-desorption was reached at 15 min). Then a certain amount of PMS (final solution containing 1 mM) was added into the above solution to trigger the degradation reaction. The solution samples were withdrawn, filtered using 0.45 μm PVDF disposable filters and injected into a vial loading with methanol at each time interval, followed by analysis with UV spectrophotometer (λ_{max} =357 nm) and high-performance liquid chromatograph (HPLC, Agilent, Waldbronn, Germany) at detecting λ of 355 nm.

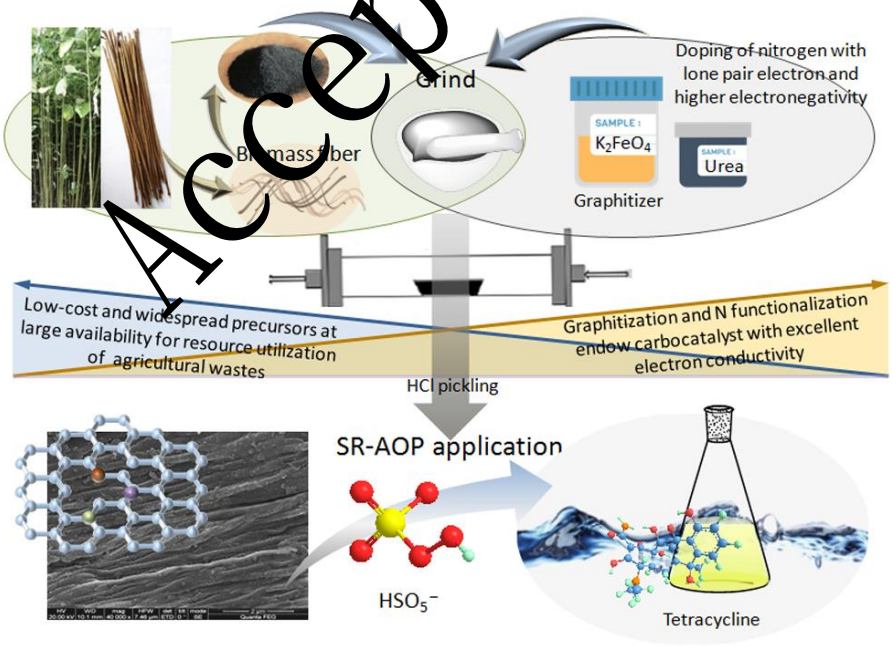

Scheme 1. Schematic illustration of the synthesis of PGBF-N as biochar-based catalyst for TC degradation.

3. Results and discussion

3.1 Characterization of biochar-based catalysts

SEM images of PGBF-N with different magnifications are shown in Fig. 1 to display the morphologies and microstructures. In the overall view of the low-resolution SEM image, the final material exhibited rod-like microstructure with an average diameter of around 50 μm, which was found to be consisted of plentiful twisted strips with diameters of about 250 nm (Fig. 1c). The intertwined like-fibrous framework, inherited from the natural morphology of biomass fiber of Ramie, should allow for effective electron transfer and mass diffusion during catalysis. The relatively rough surface with some small bumps on beam was derived from minerals in biomass after pyrolysis, in line with the observation reported in XRD. For comparison, SEM images of other carbocatalysts are also given in Fig. S1, all materials retained the inherent morphology of biomass fiber of slender column. There was little difference in morphology between RF and BF-N with a rough surface. More smooth and porous structure was formed on PGBF after modification, which was owing to the activation of KOH (hydrolyzed by K_2FeO_4) to produce gas (CO and CO_2) for pore-creating. The distinct lattice fringes with interlayer spacing of ~0.34 nm were observed in the high-resolution TEM (HRTEM) image of PGBF-N (Fig. 1e and f), which matched well with that of the (002) plane of graphite [27]. Compared with the disordered lattice on HRTEM image of pristine biochar (Fig. S2), the regular lattice arrangement further

174 demonstrated the high degree of graphitization of PGBF-N.

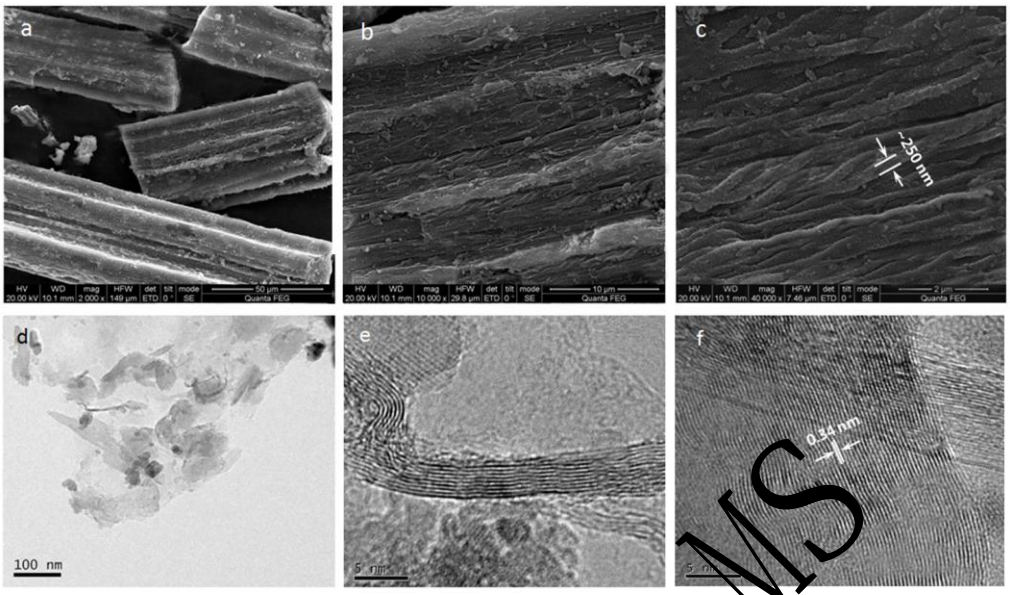

175

176 **Fig. 1** SEM images (a, b and c) and high-resolution TEM images (d, e, and f) of

177 PGBF-N.

178

179 A broad peak was observed in wide-angle X-ray diffraction pattern of BF (Fig. 2a),

180 showing the amorphous feature and no peaks that were indicative of crystalline phases

181 in carbon structure of pristine biochar. Upon modification with K_2FeO_4 followed by

182 thermal treatment, two obvious diffraction peaks at 26.3 ° and 44.1 ° which were

183 corresponding to the representative d-spacing (002) and in-plane (100) structure could

184 be observed, revealing the present of crystalline planes of graphite carbon [21]. On the

185 basis of the comparison among the XRD patterns, it could be concluded that catalytic

186 activation of K_2FeO_4 in preparation was likely to inspire the improvement of

187 graphitization degree (PGBF), as well as slight effect on crystallinity of samples by

188 nitrogen doping in PGBF-N. Several unexpected peaks at ~33 ° and ~64 ° are ascribed

189 to the crystalline minerals of calcite (PDF-# 05-0586) and quartz (PDF-# 46-1045) that
190 converted from impurities in biomass.

191 Figure S4 shows the adsorption-desorption isotherm measured at 77 K to examine
192 the textural characteristics of the synthesized biochar-based catalysts. An IV-type
193 isothermal curve as well as a large H4-type hysteretic loop of desorption branch could
194 be observed, which indicated the characteristic of mesoporous and stack structure of
195 the slit pore. Mesoporous formation is designed to the sectional decomposition and
196 conversion of amorphous carbon to denser graphitic carbon by the thermal annealing
197 process [11, 42], in which the modulation and transformation of sp^3 C cause skeleton
198 collapse and defective edge restructure. The pore size distribution, originated from
199 desorption branch and calculated by the BJH model, demonstrated an average pore size
200 of 3.953 nm in PGBF-N, with the total pore volume up to 0.096 cm^3/g. The BET
201 specific surface area (SSA) of PGBF-N was calculated to be about 81.243 m^2/g, which
202 might be appropriate balance between mass transfer and conductivity, since porosity
203 and graphitization tend to be inversely proportional. Appropriate SSA and pore
204 distribution are conducive to exposing more reaction sites for substrate contact and
205 catalysis without destroying electron conduction.

206 The graphitic structure of carbon matrix was also demonstrated by Raman
207 spectroscopy as shown in Fig. 2b. Typical D band (~1350 cm^{-1}) related to the defect
208 sites or disordered carbons, and G band (~1585 cm^{-1}) associated with E_{2g} mode
209 stretching vibration of the honeycomb-like sp^2-hybridized carbon network of graphite

were observed. The intensity ratio of I_D/I_G for BF was calculated to be 1.092, indicating the disorientated carbon structure in pristine biochar. The decreased I_D/I_G ratio to 0.982, as well as an intense 2D band (at about 2700 cm^{-1}) assigned to the two-phonon double resonance was observed in PGBF which was modified with catalysis of K_2FeO_4 in preparation, confirming the promotion of graphitization. For graphitization, amorphous Fe species were firstly reduced to metallic Fe [27] which played catalytic role for transformation of carbon configuration, as following: 1) dissolution-precipitation mechanism, in which the dispersed carbon in molten salts at high temperature transfer freely to the surface of iron particles and reconstructed as graphitic carbon on it [6]; and 2) carbide decomposition mechanism, in which the carbon atoms could be decomposed from the carbide intermediate, Fe_3C layers (metallic carbide), at higher temperature to form graphitic carbon layer [43]. Incorporation of nitrogen into hexagonal carbon induced downshift of the G peak and slight increase of I_D/I_G ratio in PGBF-N compared with PGBF, which might be attributed to the more defective sites density and edge plane exposures from N doping [11].

To further explore the surface chemical composition and the valence state of elements in biochar-based catalysts, X-ray photoelectron spectroscopy was performed and analyzed. Besides the fairly low O/C atomic ratio (8.09%), extra nitrogen (2.12 at.%) was observed in the full survey of PGBF-N (Fig. 2c), indicating the successful incorporation of nitrogen element into carbon skeleton. The high-resolution spectra of

the N1s region in Fig. 2f can be deconvoluted into main three components at binding energies of 398.40, 399.60 and 400.75 eV, corresponding to pyridinic N, pyrrolic N, and graphitic N, respectively. N-bonding configuration with high proportion of graphitic N is owing to the conversion from the pyridinic/pyrrolic N to graphitic N at annealing temperature since the substitutional heteroatoms within graphitic lattice have greater thermostability than that doped in non-hexatomic ring [23].

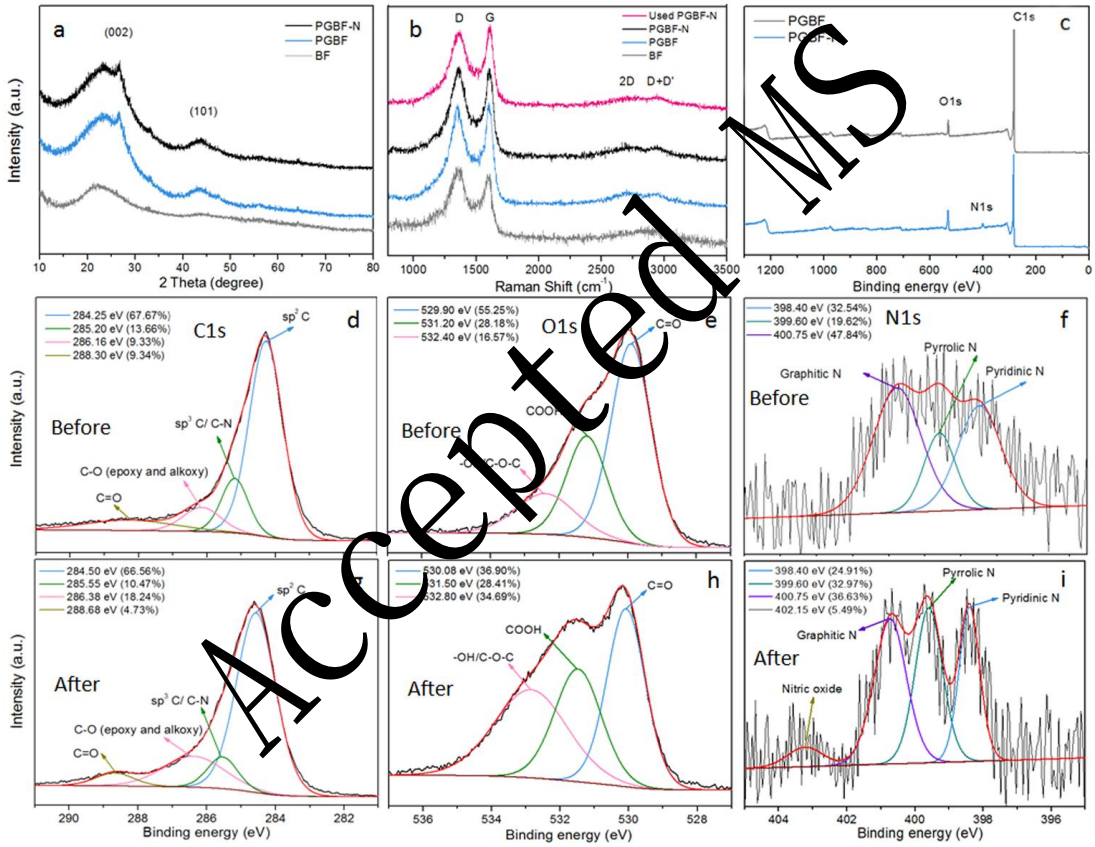

Fig. 2 XRD patterns of BF, PGBF, and PGBF-N **(**a); Raman spectra of BF, PGBF, PGBF-N, and used PGBF-N (b); XPS survey spectra of PGBF, PGBF-N (c); High resolution XPS spectrum of C 1s (d and g), O 1s (e and h); and N 1s (f and i) of PGBF-N before and after reaction.

The surface functional groups in carbocatalysts were also confirmed by FTIR spectroscopy (Fig. S5), in which several characteristic peaks of porous graphitic carbon were observed including 1637 cm^{-1} assigned to the skeletal vibration of C=C bonds in aromatic ring, 1470 cm^{-1} ascribed to ketonic C=O stretching vibration, 1385 cm^{-1} attributed to the stretching vibration of the C–C benzenoid ring, and 1072 cm^{-1} designed to C–O (alkoxy) stretching vibration. Upon treatment with nitrogen doping, the new stretch at 2262 and 1271 cm^{-1} can be originated from the conjugated triple bond of carbon-nitrogen and coupling of the C–N, respectively. These results are consistent with the observation from the high resolution XPS spectrum of C1s and O1s (Fig. 2).

3.2 Catalytic performances of biochar-based catalysts

Catalytic activities of the as-prepared biochar-based catalysts were evaluated by activating PMS for TC degradation. Fig. 3a shows a slight TC removal by only PMS degradation as well as insignificant adsorption by PGBF-N alone, indicating that most of the TC decrease comes from degradation through PMS activated by biochar-based catalyst. The degradation rate constant, k_{obs}, is assessed to gain more insight on the quantitative characterization of TC degradation by fitting with $\ln(C_0/C) = k_{obs}\, t$ (C_0: the initial TC concentration, and C_t: the TC concentration at contact time t), and corresponding results are shown in Table 1. Unmodified BF, without graphitization and nitrogen hybridization, exhibited a certain catalytic efficiency of 48.3%, which was

owing to the activation by versatile functional groups and persistent free radicals (PFRs) formed in biochar [44]. PMS activation was enhanced by biochar-based catalyst that undergone graphitization, as high as 89.1% TC removal obtained in treatment of PGBF. Graphitic-based materials with uniformly honeycomb-like carbon framework (sp^2-hybridized C) possess abundant π-electrons, whose chemical inertness could be disrupted by introducing vacancies and defects for delocalized-electron flow and transfer to trigger catalysis. However, the biochar composition is tanglesome with amorphous carbon domination. Even with a large number of edge defects reflected by I_D/I_G, pristine biochar cannot cause the directional flow of electrons, implying that only the vacancies and defects constructed on boundaries of well-organized carbon matrix showed desired catalytic properties. PGBF was observed by a lower I_D/I_G ratio along with graphitization, indicating the more excellent electron conduction ability to activate PMS than BF. On this basis, the incorporation of nitrogen atoms with lone pair electrons and high electronegativity can not only enhance electron density, but also induce electron rearrangement by conjugation with sp^2-hybridized C to accelerate electron delocalization. Although nitrogen doping reduced TC adsorption due to the decreased π-π stacking interaction between graphitic basal plane in carbon material and contaminants [23], PGBF-N displayed outstanding degradation capacity with k_{obs} of 0.0206 min^{-1} and removal efficiency of 96.5%. However, only slight changes were observed between the treatment of BF-N and BF, indicating that the nitrogen doping on the disordered carbon was of little significance, which once again confirmed the

critical role of graphitization in synthesis process for biochar-based catalyst on their activation of PMS. In addition, the excess functional groups (e.g. C–OH, amorphous C, and pyridine N) on the BF-N could be regarded as PMS and radical scavengers [11], thus resulting in less available PMS and reactive species for efficient TC degradation.

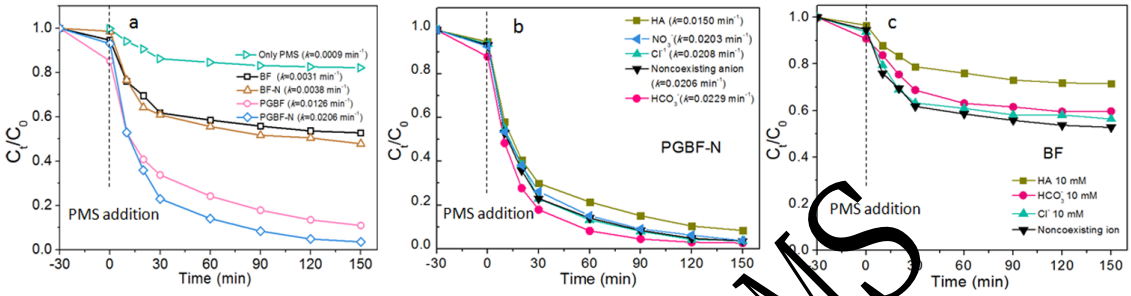

Fig. 3 Removal of TC in the presence of different biochar-based catalysts in PMS system (a); Effect of coexisting organics and inorganics on the degradation of TC in PGBF-N/PMS system (b) and BF/PMS system (c). Conditions: [biochar fiber]=0.1 g/L, [PMS]=1 mM, [temperature]=25 ℃, [TC]=20 mg/L.

Additionally, the possible intermediates of TC were identified by HPLC-MS for deeper understanding of the degradation process, and several products (the MS spectra shown on Fig. S6) and probable two TC degradation pathways were proposed and elaborated in Scheme 2. P1 (m/z =431) and P2 (m/z =417) were generated from the demethylation of the dimethylamino group in TC. Subsequently, P2 was fragmented into P3 (by deamidation), P4 (by ring opening and dealcoholization), and P5 (by deacetylation) step by step. Pathway II mainly included dehydration, hydroxylation, and fragmentation through attack by reactive species. The generation of P6 was

attributed to the dehydration and conversion of amide group to aldehyde group on P1, while P7 was produced by dehydration and hydroxylation on P2. Subsequently, P8 was obtained by deacetalization of P6 and dealcoholization of P7. P8 was decomposed into P9 via cleavage of the carboatomic ring, followed by the decarboxylation of P9 to form P10. These intermediate products were then further fragmented and produced carbon dioxide and water, which was consistent with the observation from the maximum TOC removal of 61.86% by PGBF-N (Fig. S7).

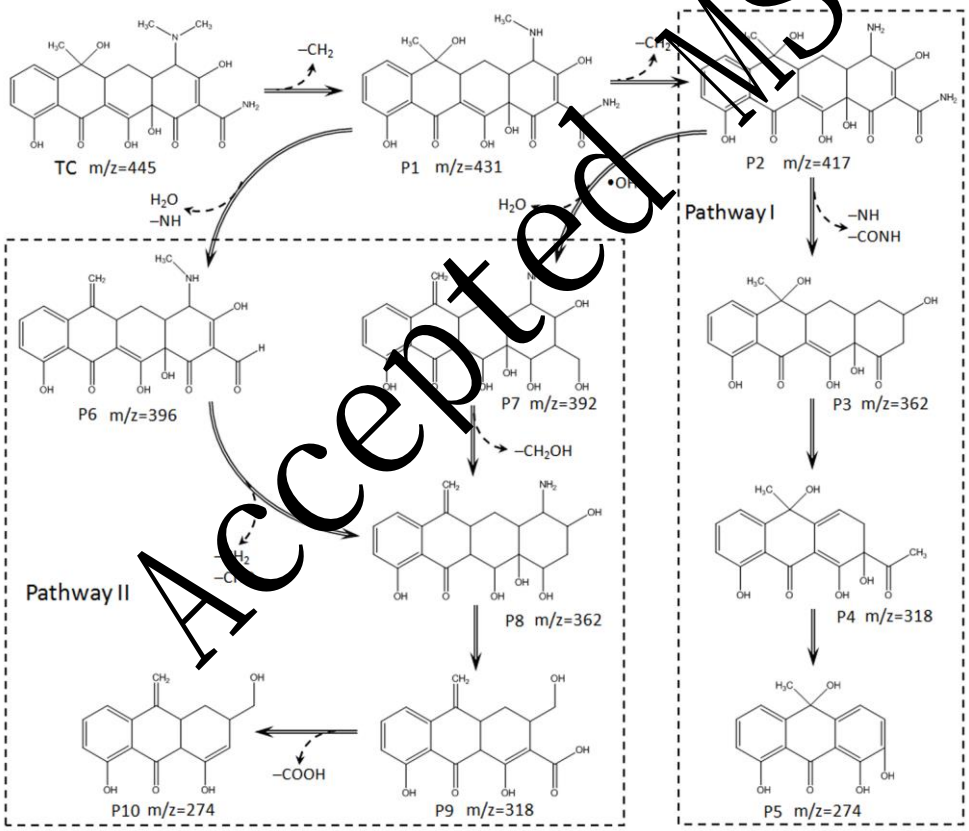

Scheme 2. Possible intermediates and proposed transformation degradation pathways of TC in PGBF-N/PMS system.

3.3 Catalytic mechanisms

Methanol (MeOH) and *tert*-butyl-alcohol (TBA) were employed as scavengers for both sulfate and hydroxyl radicals, and hydroxyl radicals, respectively. Fig. 4c shows an insignificant quenching ability on PGBF-N/PMS system even with high-ratio radical scavengers. Unexpectedly, TBA exhibited a slightly higher inhibiting impact on TC degradation than methanol, due to the hydrophobic interaction on catalyst surface impeding further surface reactions [16]. It can be inferred that free radicals (without long lifetime and long-distance migration) are generated and performed oxidation degradation on the catalyst surface. Based on this result, the more hydrophobic scavengers, phenol ($k_{SO4\bullet-+phenol}$ =8.8×10^9 M^{-1} s^{-1}, $k_{HO\bullet+phenol}$=6.6×10^9 M^{-1} s^{-1}) and nitrobenzene (NB, $k_{HO\bullet+NB}$ (3.9×10^9 M^{-1} s^{-1}) >> $k_{SO4\bullet-+NB}$ (<10^6 M^{-1} s^{-1})), were selected to terminate the surface free radical reaction. The evident decreases of TC removal percentage could be found in the present of phenol and NB of 100 mM, with the k_{obs} declining from 0.0206 min^{-1} to 0.0052 min^{-1} and 0.0066 min^{-1} (Table 1), respectively, nevertheless the removal of TC still proceeded even when radicals were captured. These results illustrated that both $SO_4\bullet^-$ and •OH were generated and participated in the reaction for certain degree of degradation, which also implied the more predominant role of non-radical pathway in TC degradation. The singlet oxygen ($^1O_2$), as a potential reactive oxygen species in non-radical pathway, was confirmed by quenching experiments with sodium azide (NaN_3) and L-histidine at 10 mM. Results in Fig. 4c showed that both NaN_3 and L-histidine led to inhibition of TC degradation, as the calculated reaction k_{obs} decreased to 0.0064 and 0.0078 min^{-1}, respectively. The

existence of $^1O_2$ was preliminarily proved, and $^1O_2$ accounted for a certain degree of TC decomposition. On the other hand, almost complete inhibiting effect was observed in the BF with phenol (Fig. 4a), indicating the absolute dominant role of the free radical pathway in group of pristine biochar. On the contrary, the calculated degradation rates in Table 1 demonstrated that PGBF (Fig. 4b) undergone graphitization had potential in carbon-bridge mediated oxidation, which was reflected by a large degradation of TC under various scavengers. While considering the consumption of PMS molecules by L-histidine, it might be concluded that reactive species $^1O_2$ played a limited role in PGBF/PMS system, although TC degradation was inhibited with rate drop from 0.0126 to 0.0075 min^{-1}. As to the graphitization and nitrogen doping in PGBF-N, graphitic nitrogen bound onto the sp^2-hybridized carbon was strongly electronegative thereby attracted electrons from adjacent carbon networks, inducing the neighboring carbon atoms to be positively charged, which was conducive to mediating the formation of $^1O_2$ by nucleophilic reaction of PMS molecules. The nucleophilic PMS molecules released electrons toward positively charged carbon atoms and partial electrophilic groups to form anion $SO_5^{\bullet -}$ radicals (Eq. 1). $^1O_2$ was generated by the self-reaction of $SO_5^{\bullet -}$ which possessed high reaction rate and low activation energy [16]. The phenomenon of radical quenching test suggested that modification with graphitization and nitrogen functionalization might induce the predominant pathway of pollutant degradation to achieve transition from radical pathway to non-radical pathway.

$$HSO_5^- \rightarrow SO_5\bullet^- + H^+ + e^- \quad (1)$$

$$SO_5\bullet^- + SO_5\bullet^- \rightarrow S_2O_8^{2-} + {}^1O_2 \quad (2)$$

$$SO_5\bullet^- + SO_5\bullet^- \rightarrow 2SO_4^- + {}^1O_2 \quad (3)$$

$$HSO_5^- + e^- \rightarrow \bullet OH + SO_4^{2-} \quad (4)$$

$$HSO_5^- + e^- \rightarrow SO_4\bullet^- + OH^- \quad (5)$$

$$SO_4\bullet^- + H_2O \rightarrow \bullet OH + SO_4^{2-} + H^+ \quad (6)$$

$$TC + \text{metastable PMS} \rightarrow \text{Intermediates} \rightarrow H_2O + CO_2 \quad (7)$$

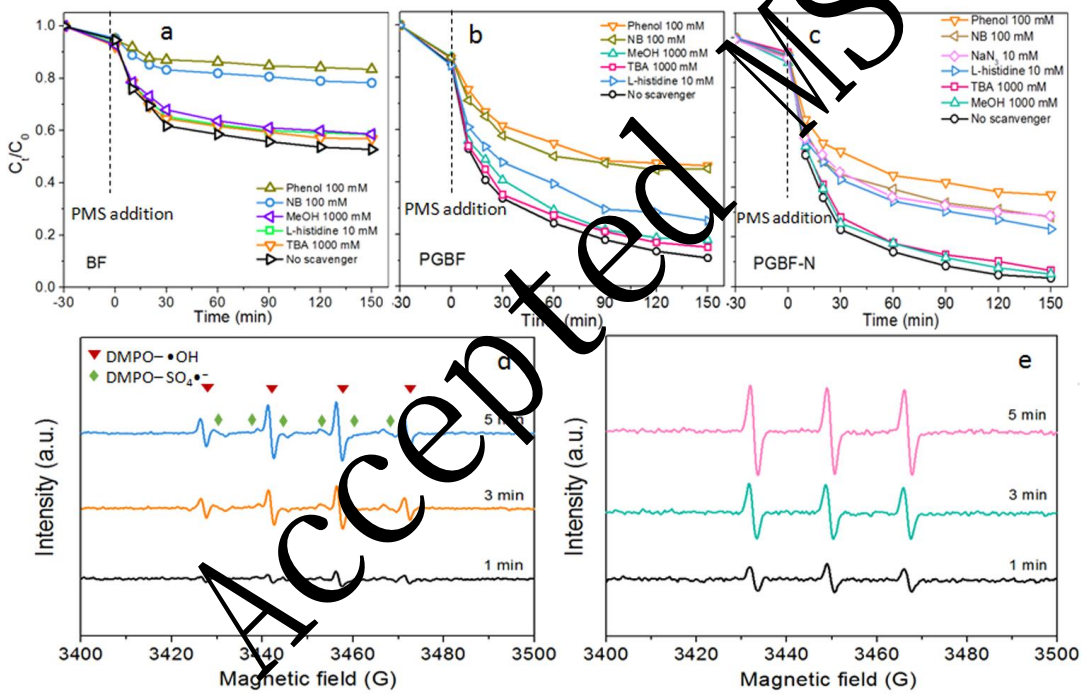

Fig. 4 Quenching experiments of BF (a), PGBF (b), and PGBF-N (c) in PMS system under different scavengers; and EPR spectrum of species adducts trapped by DMPO (d) and TEMP (e) in PMS/PGBF-N system. Conditions: [biochar fiber]=0.1 g/L, [PMS]=1 mM, [temperature]=25 ℃, [TC]=20 mg/L.

However, due to the stronger attraction between scavenger and catalyst surface

through hydrophobic force, the substance covering could further affect the interaction between PMS or TC and catalyst surface and exaggerate the quenching effect, revealing it is not rigorous to get the conclusion only by radical quenching experiment. Electron paramagnetic resonance (EPR) was applied as a powerful tool to further probe the generation and revolution processes of main reactive species on PGBF-N/PMS system, in which DMPO and TEMP were treated as spin trapping agents to trap the generated species for subsequent detection. As shown in Fig. 4d, the EPR results provided evidence of the presence of DMPO-SO_4•$^-$ and DMPO-•OH adducts in characteristic signals, and revealed that both radicals were generated immediately in the first few minutes, then a gradual revolution from SO_4•$^-$ to •OH with time accounted for the higher intensity of DMPO-•OH signal. When TEMP was used as the spin trapping agent, an obvious typical three-peak signal (a_N=17.0 G) with equal intensity, assigned to TEMPO, was observed with an increasing trend of the signal intensities as the reaction proceeded, suggesting that $^1O_2$ might be the dominant reactive species responsible for TC degradation.

To gain more insight on the non-radical pathway for TC degradation, the distinction between reactive species-dominated oxidation and carbon-bridged mediated oxidation could be draw by delayed adding contaminants at different time intervals after mixing the carbocatalyst and PMS. The reactive species with considerably short lifetime are produced on the catalyst surface once the PMS molecules are close and attached onto the surface. If the interaction between the biochar-based catalyst and

PMS is more prone to species production, a longer time interval for delayed adding contaminants will lead to a remarkable decrease in degradation efficiency due to the constant consumption of oxidizing species. It was worthwhile mentioning that the removal rate of TC decreased a little as the increased time interval for delayed adding contaminants, since it still remained at a high removal level of 70% at 9 minute intervals (Fig. 5a, Table 2), indicating the rather high contribution of TC degradation came from the bridged-role of biochar-based catalyst for electron transfer, that is, the non-radical pathway dominated by carbon-bridge oxidation was identified as the most contributory degradation pathway. The PMS molecules pre-adsorbed on the sp^2-hybridized structure of the biochar-based catalyst were activated to a metastable state since the O–O bond was weakened by electron arrangement with carbon framework. Once the electron-rich pollutants were added, the redox reaction occurred directly between pollutant molecule as an electron donor and the metastable PMS as electron acceptor with the help of PGBF-N. On the basis of the results, it can be concluded that the PGBF-N could be treated as an electron mediator to promote the electron transfer from pollutants to the PMS molecules for achieving pollutant oxidation. The same operation was carried out by catalyst of PGBF, and larger inhibition of TC removal was observed with smaller value of k_{obs}, indicating that the electron-bridged effect of PBGF was not as good as that of PGBF-N. These results implied that incorporation of nitrogen with highly electronegative into sp^2-hybridized C might inspire more metastable PMS by electron readjustment to weaken O–O bond

for pollutant degradation through electron-bridged oxidation, which also could be attributed to the increase in surface polarity and conductivity of the carbon material by nitrogen incorporation, making the surface more susceptible to interaction with polar substances. Compared with the significant inhibiting effect of adding pollutants at different time intervals in treatment of BF, it illustrated the important role of sp^2-hybridized carbon proportion, namely the graphitization degree, on the carbon-bridged oxidation of TC.

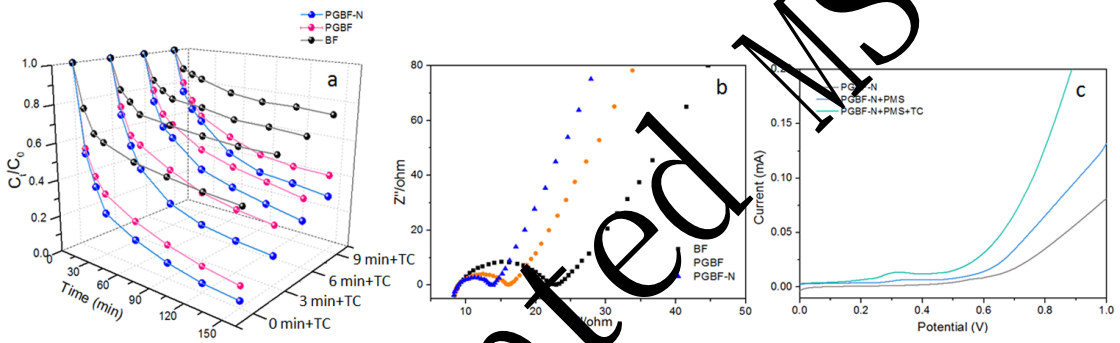

Fig. 5 The removal efficiency of TC under different regular time intervals for pollutant adding after carbocatalysts and PMS mixing (a); EIS measurement of biochar-based catalysts loaded on GCEs with frequency range from 10^{-1} to 10^5 Hz ([Na_2SO_4] =0.5 M); Linear-sweep voltammograms under different conditions (1 mM PS or both 1 mM PS and 20 mg/L TC) at a scan rate of 5 mV s^{-1} from 0.1 to 1.0 V (c).

To shed light on the electron-transfer process from pollutants to metastable PMS-carbon complexes, the conduction of biochar-based catalyst was elucidated by electrochemical measurements. The impedance of carbocatalyst is one of the important factors affecting the electron transfer, which could be provided from Nyquist plots in

EIS measurement based on the diameter of the semicircle [21, 35]. The smallest semicircle diameter is detected by PGBF-N shown in Fig. 5b, revealing the most excellent electronic conductivity of PGBF-N compared with that of BF and PGBF. In addition, the LSV plot (Fig. 5c) obtained in PGBF-N was observed by an increased current in terms of solution with 1 mM PMS, implying the interaction and electron rearrangement between PMS with biochar-based catalyst. It was worthwhile mentioning that the subsequent injection of TC led to another current enhancement, demonstrating the rapid electron transfer on the established ternary system of PMS/PGBF-N/TC, in which current flow formed on PBGF-N as bridge to facilitate electron transfer from TC molecules to metastable PMS. Mechanisms of PMS activation by PGBF-N for degradation behavior of TC molecules described above are presented in detail by Scheme 3. Besides the PMS molecules gaining electrons to generate free radicals, the positive charge on the adjacent carbon of graphite nitrogen induces the PMS molecules to lose electrons to produce $^1O_2$ through nucleophilic reactions. Direct electron transfer pathway also exists, because the promoted graphitization with increased sp^2-hybridized carbon shows more superior electric conductivity than sp^3-hybridized ones. The metastable PMS molecules that attracted on the biochar surface take electrons from TC molecules through the electron bridge role of PGBF-N to achieve the purpose of TC decomposition.

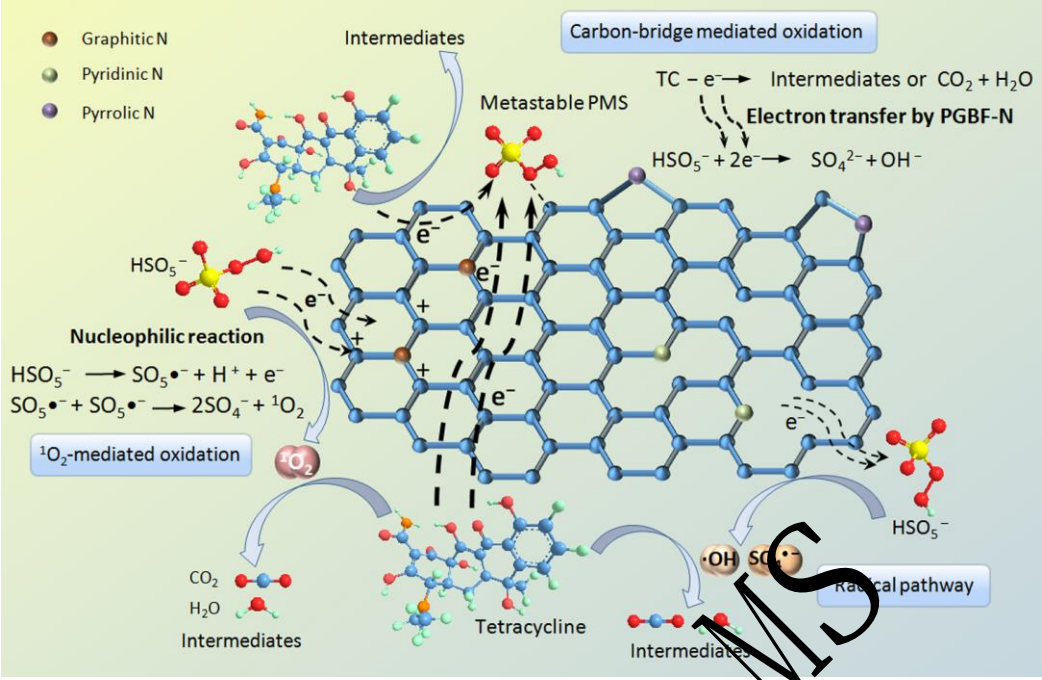

Scheme 3. Proposed mechanism of PMS activation by PGBF-N for degradation behavior of TC molecules.

3.4 Active site of PGBF-N in catalysis

The essence of catalytic activation of PMS (HO–SO_4) involves in the weakening and breaking of the superoxide O–O bond and realizing the electron transfer between catalyst and PMS molecules. In order to centralize electron density and destruct the chemical inertness of sp^2-hybridized carbon network for electron flow, several active sites, including vacancies and defects (zigzag/armchair edges) with delocalized π-electrons, versatile functional groups with lone pair electrons, and sp^2-hybridized C atom activated by conjugation with heteroatoms, were discussed for PMS activation. Electron-rich oxygen groups terminated at the defective edges were reported to be more reactive than (001) plane of graphene to achieve PMS activation [45, 46]. The

high-resolution spectrum of O1s presented in Fig. 2 (e, and h) was received to show the details of versatile oxygen functional groups on PGBF-N before and after heterogeneous catalysis. There were three fitted peaks in O1s spectrum centering at ~530.0, ~531.3 and ~532.6 eV, which were referred to the binding of C=O (ketonic group), COOH (carboxyl), and H–O/O–C–O (epoxy and alkoxy), respectively. The simultaneous and opposing changes of content proportion between ketonic C=O and O–C–O could be found in both C1s and O1s scans after catalysis, implying the conversion from ketonic C=O to C–OH/O–C–O moieties in the catalytic process, which was in good consistent with the FITR result (Fig. S5). Taking the phenomena in stability test into account, it can be inferred that the ketonic C=O as the Lewis basic sites with lone-pair electrons was more likely to effectively increase the electron density of the neighboring carbon ring and initiate the redox reaction.

Concerning to the heteroatom doping site, total N content of PGBF-N shows a negligible reduction after catalytic reaction, while an evident reconstruction of N bonding configuration analyzed by XPS can be obtained in the used carbocatalyst (Fig. 2 f, and i). It should be noted that N1s high-resolution spectrum displayed the decrease of graphitic N (from 47.84% to 36.63%) and pyridinic N (from 32.54% to 24.91%), along with the synchronized increase of pyrrolic N (from 19.62% to 32.97%), indicating the graphitic N and pyridinic N might be treated as potential active site for PMS activation and TC degradation. Because graphitic N has the greatest potential to accelerate the transfer of electrons from adjacent carbon atoms and effectively destroy

485 the inertness of conjugated graphitic carbon network [11, 22], the increase in positive
486 charge of carbon atoms caused by graphitic N is conducive to weakening O–O bonds
487 to form surfaced metastable PMS by electron rearrangement or generate reactive
488 substances ($^1O_2$) through nucleophilic addition reaction of PMS toward positively
489 charged carbon.

490 In addition to the versatile oxygen functional groups and heteroatom doping, the
491 imperfect hexagonal units with vacancies, zigzag/armchair edges incorporated on
492 sp^2-carbon lattice were also well demonstrated to be served as active sites in
493 heterogeneous catalysis [12, 23, 47]. The defective edge at the boundary of
494 sp^2-hybridize C framework, originated from crack of the perfect honeycomb unit, has a
495 closer Femi level to the bulk structure and unique electronic state of dangling σ bonds
496 with unconfined π-electrons, thereby showing excellent catalytic properties. Notably,
497 there is no significantly improved removal rate of TC between treatment of BF and
498 BF-N, suggesting that it is meaningless by nitrogen doping on pristine biochar. For
499 biochar systems with a fairly complex composition, the formation of sp^2-hybridize
500 carbon is critical, because the defects formed in hexagonal graphitic carbon network
501 are conducive to electron transfer. The doping of heteroatoms on the disorientated
502 system can just increase the intricacy but cannot effectively orient the electrons for
503 achieving redox reaction.

504

505 **3.5 Catalyst recyclability and its application on real water samples**

To further explore the practical application, the effects of several common matrix species on catalytic performance of biochar fiber were investigated systematically. Previous research including the results of BF in this study (Fig. 3c) revealed the inhibitory effect of some common inorganic species, which was attributed to the reaction with sulfate and hydroxyl radicals to generate weaker radical species [48] While results shown in Fig. 3b demonstrated little inhibiting effect of usual anions (e.g. Cl^-, NO_3^-) on TC degradation within 10 mM, indicating TC degradation by PGBF-N was dominated by non-radical pathway which could avoid radical quenching reaction and suffer less interference from background substances in water. One unanticipated finding was that the addition of HCO_3^- at 10 mM in present study promoted PMS decomposition and TC degradation, which was different from those papers reported that HCO_3^- served as a scavenger to reduce the degradation efficiency [35]. This might be attributed to the buffering action of HCO_3^- kept the solution alkaline throughout the reaction, where an alkaline environment would benefit dissociation of HSO_5^- into SO_5^{2-} and provide more opportunities for inducing $^1O_2$ evolution in non-radical pathway through Eq. 8 [49], coinciding with the pH test that alkaline environment enhanced the removal rate of TC (Fig. S9). Qiu et al. (2019) also reported a synergistic effect of bicarbonate/MNCs/PMS, in which the generated carbonate radicals inspired the formation of HO_2•, thereby promoting the $^1O_2$ generation through a series of chain reactions (Eqs. 9-13) [50]. Different results of ion interference from various studies may be ascribed to different predominant reactive species and molecular structures of

pollutants.

$HSO_5^- + SO_5^{2-} \rightarrow HSO_4^- + SO_4^{2-} + {}^1O_2$ (8)

$HSO_5^- + H_2O \rightarrow H_2O_2 + HSO_4^-$ (9)

$SO_5^{2-} + H_2O \rightarrow H_2O_2 + SO_4^{2-}$ (10)

$H_2O_2 + CO_3^{\bullet -} \rightarrow HCO_3^- + HO_2^{\bullet}$ (11)

$H_2O_2 + {}^{\bullet}OH \rightarrow H_2O + HO_2^{\bullet}$ (12)

$HO_2^{\bullet} + HO_2^{\bullet} \rightarrow H_2O_2 + {}^1O_2$ (13)

In order to deeply investigate the practical application of biochar-based catalysts in actual natural water, tap water, river water and pharmaceutical wastewater containing various organic and inorganic compounds in different contents (characteristics shown in Table S1) were employed as medium of TC solution in comparison with deionized water. Results of TC degradation efficiency in Fig. 6a showed similar trend obtained from tap water and deionized water. Based on differences in water characteristics, the higher levels of organic matter make negligible negative effect on TC degradation, which implied the weak competitiveness of natural organic matters on reactive activity with $^1O_2$, and weak electron-donating ability of organic matters for triggering carbon-bridged oxidation, taking into account the insignificant content of inorganic compounds. As to the treatments in the medium of river water and pharmaceutical water, higher adsorption capacity of PGBF-N for TC was observed due to the adhesion and encapsulation by suspended particles and colloids. However, a large amount of

548 reducing substances, reflected by the high COD value (Table S1), make competition
549 for consumption of PMS and reactive substances, accounting for the decline of
550 degradation rate in pharmaceutical water.

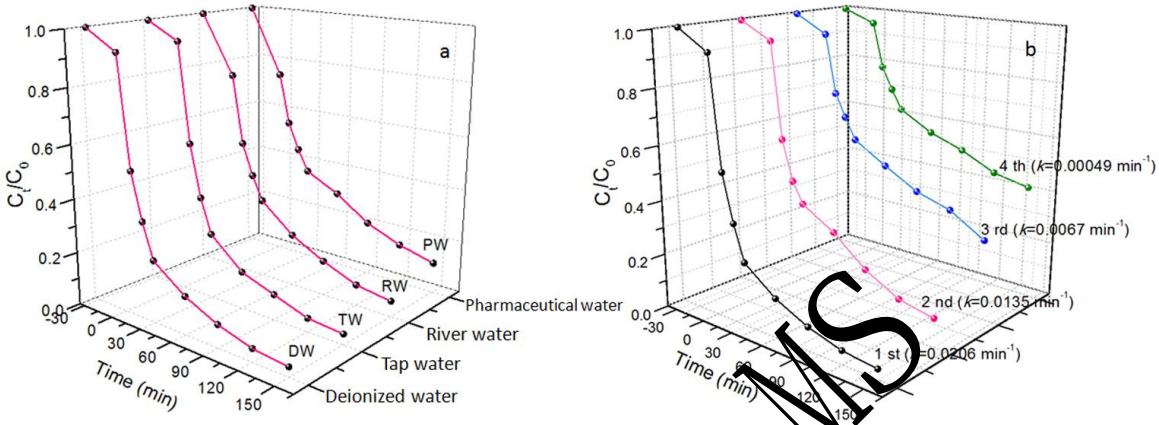

551

552 **Fig. 6** Degradation for TC removal in different water samples (a) and Cycling
553 performance (b) by PGBF-N/PMS system. Conditions: [PGBF-N]=0.1 g/L, [PMS]=1
554 mM, [temperature]=25 ℃, [TC]=20 mg/L.

555

556 The recycling experiments were performed on four-cycles to evaluate the
557 reusability and stability of the biochar-based catalysts in PMS system for TC removal.
558 Results presented in Fig. 6b demonstrated a significant decline in removal efficiency
559 by PGBF-N/PMS with approximately 60% in the fourth cycle experiment, which could
560 be resulted from the surface passivation (containing irreversible conversion of the
561 active site and cannibalistic surface oxidation reaction), and surface coverage by
562 organics [4, 16]. It was worthwhile mentioning that, on the whole, the proposed
563 PGBF-N showed a relatively good degradation and recycling performance compared
564 with other carbon materials (Table. S2), which was due to the fact that the non-radical

pathway, especially the carbon-bridged oxidation, dominated in the PGBF-N/PMS system, in which the biochar fiber acted as an electron mediator (electron transfer from PMS to contaminants) with minimizing surface passivation.

4. Conclusions

In conclusion, biomass fiber was utilized to synthesize biochar-based catalysts through modified process with graphitization and nitrogen incorporation. The prepared PGBF-N has great application potential with high catalytic degradation efficiency toward targeted pollutants dominated by non-radical pathways with enhancing electron transfer. Graphitization and nitrogen doping are proven to have the ability to increase the contribution of non-radical pathways which suffer less interference from background environment in real wastewater containing complex components. Based on the catalyst characterization results before and after the reaction, it is proposed that the electron-rich ketonic functional group, graphitic N and defect sites on carbon network are possible active sites to promote the TC degradation. These findings still open opportunities for design of metal-free catalyst on basis of the mechanistic concept that graphitization and nitrogen functionalization allow degradation mechanisms trend to non-radical pathways to overcome the negative effects of free radical.

Acknowledgments

This research was financially supported by the National Natural Science

Foundation of China (81773333, 51521006, 51809011, 51679082 and 51809089) and the Program for Changjiang Scholars and Innovative Research Team in University (IRT-13R17), the Three Gorges Follow-up Research Project (2017HXXY-05), and the Research and development plan of key areas in Hunan Province (2019NK2062).

References

[1] P. Xu, G.M. Zeng, D.L. Huang, C.L. Feng, S. Hu, M.H. Zhao, C. Lai, Z. Wei, C. Huang, G.X. Xie, Z.F. Liu, Use of iron oxide nanomaterials in wastewater treatment: A review, Sci. Total Environ. 424 (2012) 1-10.

[2] P. Duan, T. Ma, Y. Yue, Y. Li, X. Zhang, Y. Shang, B. Gao, Q. Zhang, Q. Yue, X. Xu, Fe/Mn nanoparticles encapsulated in nitrogen-doped carbon nanotubes as a peroxymonosulfate activator for acetamiprid degradation, Environ. Sci-Nano. 6 (2019) 1799-1811.

[3] P. Zhang, X.F. Tan, S.B. Liu, Y.G. Liu, G.M. Zeng, S.J. Ye, Z.H. Yin, X.J. Hu, N. Liu, Catalytic degradation of estrogen by persulfate activated with iron-doped graphitic biochar: Process variables effects and matrix effects, Chem. Eng. J. 378 (2019).

[4] S. Indrawirawan, H. Sun, X. Duan, S. Wang, Nanocarbons in different structural dimensions (0–3D) for phenol adsorption and metal-free catalytic oxidation, Appl. Catal. B-Environ. 179 (2015) 352-362.

[5] Y. Wang, H. Cao, C. Chen, Y. Xie, H. Sun, X. Duan, S. Wang, Metal-free catalytic ozonation on surface-engineered graphene: Microwave reduction and heteroatom doping, Chem. Eng. J. 355 (2019) 118-129.

[6] L. Xie, G. Sun, F. Su, X. Guo, Q. Kong, X. Li, X. Huang, L. Wan, W. Song, K. Li, C. Lv, C. Chen, Hierarchical porous carbon microtubes derived from willow catkins for supercapacitor applications. J. Mater. Chem. A. 4 (2016) 1637-1646.

[7] W.D. Oh, Z.L. Dong, T.T. Lim, Generation of sulfate radical through heterogeneous catalysis for organic contaminants removal: Current development, challenges and prospects, Appl. Catal. B-Environ. 194 (2016) 169-201.

[8] H. Wang, Z. Zeng, P. Xu, L. Li, G. Zeng, R. Xiao, Z. Tang, D. Huang, L. Tang, C. Lai, D. Jiang, Y. Liu, H. Yi, L. Qin, S. Ye, X. Ren, W. Tang, Recent progress in covalent organic framework thin films: fabrications, applications and perspectives, Chem. Soc. Rev. 48 (2019) 488-516.

[9] B. Song, M. Chen, S.J. Ye, P. Xu, G.M. Zeng, J.L. Gong, J. Li, P. Zhang, W.C. Cao, Effects of multi-walled carbon nanotubes on metabolic function of the microbial community in riverine sediment contaminated with phenanthrene, Carbon. 144 (2019) 1-7.

[10] P. Duan, Y. Qi, S. Feng, X. Peng, W. Wang, Y. Yue, Y. Shang, Y. Li, B. Gao, X. Xu, Enhanced degradation of clothianidin in Peroxymonosulfate/catalyst system via core-shell FeMn @ N-C and phosphate surrounding, Appl. Catal. B-Environ. (2020) 118717.

[11] W.D. Oh, G. Lisak, R.D. Webster, Y.N. Liang, A. Veksha, A. Giannis, J.G.S. Moo, J.W. Lim, T.T. Lim, Insights into the thermolytic transformation of lignocellulosic biomass waste to redox-active carbocatalyst: Durability of surface active sites, Appl. Catal. B-Environ. 233 (2018) 120-129.

[12] X. Duan, H. Sun, Z. Ao, L. Zhou, G. Wang, S. Wang, Unveiling the active sites of graphene-catalyzed peroxymonosulfate activation, Carbon. 107 (2016) 371-378.

[13] Y. Shang, C. Chen, P. Zhang, Q. Yue, Y. Li, B. Gao, X. Xu, Removal of sulfamethoxazole

631 from water via activation of persulfate by Fe_3C@NCNTs including mechanism of radical
632 and nonradical process, Chem. Eng. J. 375 (2019) 122004.
633 [14] J. Liu, P. Wu, S. Yang, S. Rehman, Z. Ahmed, N. Zhu, Z. Dang, Z. Liu, A photo-switch for
634 peroxydisulfatenon-radical/radical activation over layered CuFe oxide: Rational
635 degradation pathway choice for pollutants, Appl. Catal. B-Environ. 261 (2020) 118232.
636 [15] P. Shao, J. Tian, F. Yang, X. Duan, S. Gao, W. Shi, X. Luo, F. Cui, S. Luo, S. Wang,
637 Identification and regulation of active sites on nanodiamonds: Establishing a highly
638 efficient catalytic system for oxidation of organic contaminants, Adv. Func. Mater. 28
639 (2018) 1705295.
640 [16] R. Luo, M. Li, C. Wang, M. Zhang, M.A. Nasir Khan, X. Sun, J. Shen, W. Han, L. Wang,
641 J. Li, Singlet oxygen-dominated non-radical oxidation process for efficient degradation of
642 bisphenol A under high salinity condition, Water Res. 148 (2019) 416-424.
643 [17] C. Chen, T. Ma, Y. Shang, B. Gao, B. Jin, H. Dan, Q. Li, Q. Yue, Y. Li, Y. Wang, X. Xu,
644 In-situ pyrolysis of Enteromorpha as carbocatalyst for catalytic removal of organic
645 contaminants: considering the intrinsic N/Fe in Enteromorpha and non-radical reaction,
646 Appl. Catal. B-Environ. 250 (2019) 382-395.
647 [18] S. Yang, P. Wu, J. Liu, Z. Chen, Z. Ahmed, N. Zhu, Efficient removal of bisphenol A by
648 superoxide radical and singlet oxygen generated from peroxymonosulfate activated with
649 Fe0-montmorillonite, Chem. Eng. J. 350 (2018) 484-495.
650 [19] X. Du, Y. Zhang, F. Si, C. Yao, M. Du, I. Hussain, H. Kim, S. Huang, Z. Lin, W. Hayat,
651 Persulfate non-radical activation by nano-CuO for efficient removal of chlorinated organic
652 compounds: Reduced graphene oxide-assisted and CuO (0 0 1) facet-dependent, Chem.
653 Eng. J. 356 (2019) 178-189.
654 [20] X.G. Duan, Z.M. Ao, H.Q. Sun, L. Zhou, G.X. Wang, S.B. Wang, Insights into N-doping
655 in single-walled carbon nanotubes for enhanced activation of superoxides: a mechanistic
656 study, Chem. Commun. 51 (2015) 15249-15252.
657 [21] S. Zhu, X. Huang, F. Ma, L. Wang, X. Duan, S. Wang, Catalytic removal of aqueous
658 contaminants on N-doped graphitic biochars: inherent roles of adsorption and nonradical
659 mechanisms, Environ. Sci. Technol. 52 (2018) 8649-8658.
660 [22] X. Duan, C. Su, L. Zhou, H. Sun, A. Suvorova, T. Odedairo, Z. Zhu, Z. Shao, S. Wang,
661 Surface controlled generation of reactive radicals from persulfate by carbocatalysis on
662 nanodiamonds, Appl. Catal. B-Environ. 194 (2016) 7-15.
663 [23] X. Chen, W.D. Oh, Z.T. Hu, Y.M. Sun, R.D. Webster, S.Z. Li, T.T. Lim, Enhancing
664 sulfacetamide degradation by peroxymonosulfate activation with N-doped graphene
665 produced through delicately-controlled nitrogen functionalization via tweaking thermal
666 annealing processes, Appl. Catal. B-Environ. 225 (2018) 243-257.
667 [24] S. Ye, G. Zeng, H. Wu, C. Zhang, J. Dai, J. Liang, J. Yu, X. Ren, H. Yi, M. Cheng, C.
668 Zhang, Biological technologies for the remediation of co-contaminated soil, Crit. Rev.
669 Biotechnol. 37 (2017) 1062-1076.
670 [25] S.J. Ye, G.M. Zeng, H.P. Wu, J. Liang, C. Zhang, J. Dai, W.P. Xiong, B. Song, S.H. Wu,
671 J.F. Yu, The effects of activated biochar addition on remediation efficiency of
672 co-composting with contaminated wetland soil, Resour. Conserv. Recy. 140 (2019)

278-285.
[26] W. Du, Q. Zhang, Y. Shang, W. Wang, Q. Li, Q. Yue, B. Gao, X. Xu, Sulfate saturated biosorbent-derived Co-S@NC nanoarchitecture as an efficient catalyst for peroxymonosulfate activation, Appl. Catal. B-Environ. 262 (2020) 118302.
[27] Y.N. Gong, D.L. Li, C.Z. Luo, Q. Fu, C.X. Pan, Highly porous graphitic biomass carbon as advanced electrode materials for supercapacitors, Green. Chem, 19 (2017) 4132-4140.
[28] L.X. Zuo, W.J. Wang, R.B. Song, J.J. Lv, L.P. Jiang, J.J. Zhu, NaCl crystal tuning nitrogen self-doped porous graphitic carbon nanosheets for efficient oxygen reduction, Acs Sustain. Chem. Eng. 5 (2017) 10275-10282.
[29] J.S. Xia, N. Zhang, S.K. Chong, D. Li, Y. Chen, C.H. Sun, Three-dimensional porous graphene-like sheets synthesized from biocarbon via low-temperature graphitization for a supercapacitor, Green. Chem. 20 (2018) 694-700.
[30] Y. Yang, C. Zhang, C. Lai, G. Zeng, D. Huang, M. Cheng, J. Wang, F. Chen, C. Zhou, W. Xiong, BiOX (X=Cl, Br, I) photocatalytic nanomaterials: Applications for fuels and environmental management, Adv. Colloid Interf. Sci. 254 (2018) 76-93.
[31] S.J. Ye, G.M. Zeng, H.P. Wu, C. Zhang, J. Liang, J. Dai, Z.F. Liu, W.P. Xiong, J. Wan, P.A. Xu, M. Cheng, Co-occurrence and interactions of pollutants, and their impacts on soil remediation-A review, Crit. Rev. Env. Sci. Technol. 47 (2017) 1528-1553.
[32] C.Y. Zhou, C. Lai, C. Zhang, G.M. Zeng, D.L. Huang, M. Cheng, L. Hu, W.P. Xiong, M. Chen, J.J. Wang, Y. Yang, L.B. Jiang, Semiconductor/boron nitride composites: Synthesis, properties, and photocatalysis applications, Appl. Catal. B-Environ. 238 (2018) 6-18.
[33] S. Yang, Z. Huang, P. Wu, Y. Li, X. Dong, C. Li, N. Zhu, X. Duan, D. Dionysios, Rapid removal of tetrabromobisphenol A by α-Fe2O3-x@Graphene@Montmorillonite catalyst with oxygen vacancies through peroxymonosulfate activation: Role of halogen and α-hydroxyalkyl radicals, Appl. Catal. B-Environ. 260 (2020) 118129.
[34] P. Zhang, S.B. Liu, X.F. Tan, Y.G. Liu, G.M. Zeng, Z.H. Yin, S.J. Ye, Z.W. Zeng, Microwave-assisted chemical modification method for surface regulation of biochar and its application for estrogen removal, Process Saf. Environ. 128 (2019) 329-341.
[35] S.J. Ye, M. Yan, X.F. Tan, J. Liang, G.M. Zeng, H.P. Wu, B. Song, C.Y. Zhou, Y. Yang, H. Wang, Facile assembled biochar-based nanocomposite with improved graphitization for efficient photocatalytic activity driven by visible light, Appl. Catal. B-Environ. 250 (2019) 78-88.
[36] X.D. Liu, Y.C. Chen, Y.Y. Yao, Q.H. Bai, Z.W. Wu, Iodine-doped carbon fibers as an efficient metal-free catalyst to activate peroxymonosulfate for the removal of organic pollutants, Catal. Sci. Technol. 8 (2018) 5482-5489.
[37] X.F. Tan, Y.G. Liu, Y.L. Gu, S.B. Liu, G.M. Zeng, X. Cai, X.J. Hu, H. Wang, S.M. Liu, L.H. Jiang, Biochar pyrolyzed from MgAl-layered double hydroxides pre-coated ramie biomass (*Boehmeria nivea* (L.) Gaud.): Characterization and application for crystal violet removal, J Environ. Manage. 184 (2016) 85-93.
[38] K.R. Reddy, K. Maturi, C. Cameselle, Sequential Electrokinetic Remediation of Mixed Contaminants in Low Permeability Soils. J. Environ. Eng, 135(2009), 989-998.
[39] Z. Zeng, S. Ye, H. Wu, R. Xiao, G. Zeng, J. Liang, C. Zhang, J. Yu, Y. Fang, B. Song,

Research on the sustainable efficacy of g-MoS2 decorated biochar nanocomposites for removing tetracycline hydrochloride from antibiotic-polluted aqueous solution, The Sci. Total Environ. 648 (2019) 206-217.
[40] W.J. Xue, D.L. Huang, J. Li, G.M. Zeng, R. Deng, Y. Yang, S. Chen, Z.H. Li, X.M. Gong, B. Li, Assembly of AgI nanoparticles and ultrathin g-C3N4 nanosheets codecorated Bi2WO6 direct dual Z-scheme photocatalyst: An efficient, sustainable and heterogeneous catalyst with enhanced photocatalytic performance, Chem. Eng. J. 373 (2019) 1144-1157.
[41] S.J. Liu, Y.G. Liu, X.F. Tan, S.B. Liu, M.F. Li, N. Liu, Z.H. Yin, S.R. Tian, Y.H. Zhou, Facile synthesis of MnOx-loaded biochar for the removal of doxycycline hydrochloride: effects of ambient conditions and co-existing heavy metals, J Chem. Technol. Biot. 94 (2019) 2187-2197.
[42] L. Zhao, W. Zheng, X.D. Cao, Distribution and evolution of organic matter phases during biochar formation and their importance in carbon loss and pore structure, Chem. Eng. J. 250 (2014) 240-247.
[43] X.H. Zhang, K. Zhang, H.X. Li, Q. Wang, L.E. Jin, Q. Cao, Synthesis of porous graphitic carbon from biomass by one-step method And its role in the electrode for supercapacitor, J Appl. Electrochem. 48 (2018) 415-426.
[44] G. Fang, C. Liu, J. Gao, D.D. Dionysiou, D. Zhou, Manipulation of persistent free radicals in biochar to activate persulfate for contaminant degradation, Environ. Sci. Technol. 49 (2015) 5645-5653.
[45] H. Sun, C. Kwan, A. Suvorova, H.M. Ang, M.O. Tadé, S. Wang, Catalytic oxidation of organic pollutants on pristine and surface nitrogen-modified carbon nanotubes with sulfate radicals, Appl. Catal. B-Environ. 154-155 (2014) 134-141.
[46] B. Frank, J. Zhang, R. Blume, R. Schlogl, D.S. Su, Heteroatoms increase the selectivity in oxidative dehydrogenation reactions on nanocarbons, Angew. Chemie. 48 (2009) 6913-6917.
[47] X. Duan, H. Sun, J. Kang, Y. Wang, S. Indrawirawan, S. Wang, Insights into heterogeneous catalysis of persulfate activation on dimensional-structured nanocarbons, ACS Catalysis. 5 (2015) 4629-4636.
[48] L. Tang, Y.I. Liu, J.J. Wang, G.M. Zeng, Y.C. Deng, H.R. Dong, H.P. Feng, J.J. Wang, B. Peng, Enhanced activation process of persulfate by mesoporous carbon for degradation of aqueous organic pollutants: Electron transfer mechanism, Appl. Catal. B-Environ. 231 (2018) 1-10.
[49] M. Nie, W. Zhang, C. Yan, W. Xu, L. Wu, Y. Ye, Y. Hu, W. Dong, Enhanced removal of organic contaminants in water by the combination of peroxymonosulfate and carbonate, Sci. Total Environ. 647 (2019) 734-743.
[50] X. Qiu, S. Yang, M. Dzakpasu, X. Li, D. Ding, P. Jin, R. Chen, Q. Zhang, X.C. Wang, Attenuation of BPA degradation by SO4− in a system of peroxymonosulfate coupled with Mn/Fe MOF-templated catalysts and its synergism with Cl− and bicarbonate, Chem. Eng. J. 372 (2019) 605-615.

755 **Table 1. The pollutant degradation rate constants in different scavengers by**
756 **PMS/different biochar-based catalysts.**
757

Carbocatalyst		**MeOH**	**TBA**	**Phenol**	**BN**	**L-histidine**	**NaN_3**	**None**
	n[scavenger : PMS]	1000	1000	100	100	10	10	-
PGBF-N	k_{obs}, min^{-1}	0.0176	0.0161	0.0052	0.0066	0.0078	0.0064	0.0206
PGBF	k_{obs}, min^{-1}	0.0098	0.0105	0.0042	0.0051	0.0075	-	0.0126
BF	k_{obs}, min^{-1}	0.0025	0.0026	0.0007	0.0010	0.0024	-	0.0031

Table 2. The pollutant degradation rate constants at different time intervals for adding pollutants.

Time interval		Different biochar-based catalysts		
		PGBF-N	PGBF	BF-N
0 min	k_{obs} (min^{-1})	0.0207	0.0130	0.0039
3 min	k_{obs} (min^{-1})	0.0113	0.0069	0.0025
6 min	k_{obs} (min^{-1})	0.0083	0.0059	0.0019
9 min	k_{obs} (min^{-1})	0.0075	0.0053	0.0017